JACS
JOURNAL OF THE AMERICAN CHEMICAL SOCIETY
Communication
pubs.acs.org/JACS

Low-Temperature Solution-Processed Tin Oxide as an Alternative Electron Transporting Layer for Efficient Perovskite Solar Cells

Weijun Ke,[†,‡] Guojia Fang,*[,†] Qin Liu,[†] Liangbin Xiong,[†] Pingli Qin,[†] Hong Tao,[†] Jing Wang,[†] Hongwei Lei,[†] Borui Li,[†] Jiawei Wan,[†] Guang Yang,[†] and Yanfa Yan*[,‡]

[†]Key Laboratory of Artificial Micro- and Nano-structures of Ministry of Education of China, School of Physics and Technology, Wuhan University, Wuhan 430072, People's Republic of China

[‡]Department of Physics and Astronomy and Wright Center for Photovoltaics Innovation and Commercialization, The University of Toledo, Toledo, Ohio 43606, United States

Supporting Information

ABSTRACT: Lead halide perovskite solar cells with the high efficiencies typically use high-temperature processed TiO_2 as the electron transporting layers (ETLs). Here, we demonstrate that low-temperature solution-processed nanocrystalline SnO_2 can be an excellent alternative ETL material for efficient perovskite solar cells. Our best-performing planar cell using such a SnO_2 ETL has achieved an average efficiency of 16.02%, obtained from efficiencies measured from both reverse and forward voltage scans. The outstanding performance of SnO_2 ETLs is attributed to the excellent properties of nanocrystalline SnO_2 films, such as good antireflection, suitable band edge positions, and high electron mobility. The simple low-temperature process is compatible with the roll-to-roll manufacturing of low-cost perovskite solar cells on flexible substrates.

Organic−inorganic lead halide perovskite solar cells have attracted enormous attention in recent years. The power conversion efficiency (PCE) of perovskite solar cells has rapidly increased from 3.8% to 20.1% (certified) in just 6 years.[1−10] Such a rapid increase in efficiency is largely attributed to the superior photovoltaic properties of lead halide perovskites, such as the extremely high optical absorption coefficient and very long carrier lifetime.[11−14] High-efficiency perovskite solar cells typically use electron transporting layers (ETLs)/hole blocking layers and hole transporting layers (HTLs)/electron blocking layers to separate and collect photogenerated charge carriers produced in perovskite absorbers. These layers are critical for achieving high-efficiency cells because they prevent severe carrier recombination at interfaces, which may dictate the open-circuit voltages (V_{oc}'s) and fill factors (FFs) of solar cells. Perovskite solar cells without ETLs and/or HTLs have exhibited lower efficiencies as compared to the cells with ETLs and HTLs.[15,16] The electrical and optical properties of ETLs and HTLs can significantly affect the performance of perovskite solar cells. Perovskite solar cells use either regular or inverted architectures.[17−23] So far, the record efficiency cells have the regular architecture, in which light enters from the ETL and compact TiO_2 is used as the ETL material. Though the record efficiency cells use TiO_2 ETLs, the optical and electronic properties of TiO_2 still exhibit some shortfalls, making it not the ultimate ETL material. For example, the electron mobility of TiO_2 is not high enough. Zhou et al. showed that Y-doping can increase the electron mobility and electrical conductivity of TiO_2 and therefore improve the efficiencies for perovskite cells.[7] However, doping may not be able to completely overcome the intrinsic low electron mobility issue. Moreover, Snaith et al. reported that perovskite solar cells using mesoporous TiO_2 are sensitive to ultraviolet (UV) illumination.[24] There exist other transparent metal oxides, such as ZnO, In_2O_3, and SnO_2, that exhibit similar or even better electrical and optical properties as compared to TiO_2. Especially, these oxides exhibit a much higher electron mobility than TiO_2.[25] Recently, Liu et al. reported that a planar perovskite solar cell using a low-temperature solution-processed nanoparticle (ZnO) ETL achieved a high PCE of 15.7%.[26] The results suggest that metal oxides other than TiO_2 can be good ETL materials for high-efficiency perovskite solar cells. SnO_2 is a metal oxide that has not only a much higher electron mobility but also a wider band gap than TiO_2.[25,27] Because ETLs absorb photons with energies higher than the band gap but do not contribute to photocurrents, such absorptions cause only a small current loss. Therefore, SnO_2 should lead to a smaller ETL-induced current loss than TiO_2. For ultra-high-efficiency cells, every potential energy loss should be eliminated. Moreover, SnO_2, with a wider band gap, is more stable than TiO_2 under UV illumination.[25] Fluorine-doped SnO_2 (FTO) is a robust transparent conducting electrode that has been widely used in the thin-film solar cell industry. Gelled SnO_2 nanoparticles have been used as ETLs for polymer-based solar cells.[28] Dye-sensitized solar cells using high-temperature prepared mesoporous SnO_2 particles coated with TiO_2 and MgO have achieved high efficiencies.[27] However, there is no report on efficient perovskite solar cells using SnO_2 as both ETLs and antireflection films.

Here, we report on low-cost and low-temperature solution-processed SnO_2 as an ETL material for achieving highly efficient planar perovskite solar cells. The best-performing planar cell using a SnO_2 ETL has achieved PCEs of 17.21% and 14.82% when measured under reverse and forward voltage scans, respectively. The perovskite solar cells using SnO_2 ETLs

Received: February 23, 2015
Published: May 19, 2015

DOI: 10.1021/jacs.5b01994
J. Am. Chem. Soc. 2015, 137, 6730−6733

exhibited high PCEs, V_{oc}'s, and short-circuit currents (J_{sc}'s), attributed to the excellent optical and electrical properties of nanocrystalline SnO_2—wide band gap, good antireflection, and high electron mobility. Our results, therefore, suggest that low-temperature processed SnO_2 is an excellent alternative ETL material for efficient perovskite solar cells. The low-temperature processed SnO_2 provides a new opportunity for further improving the performance of perovskite solar cells. Furthermore, the low-temperature process is compatible with the roll-to-roll manufacturing of perovskite solar cells on flexible substrates.

In this study, the SnO_2 ETLs were synthesized by a facile solution approach—spin-coating of $SnCl_2{\cdot}2H_2O$ precursor prepared at a room temperature and followed by thermal annealing in air at 180 °C for 1 h. The ETLs were treated by UV−ozone for 15 min before perovskite synthesis. Because SnO_2 thin films are used as ETLs, our perovskite solar cells have the regular cell architecture, as shown in Figure 1a. The

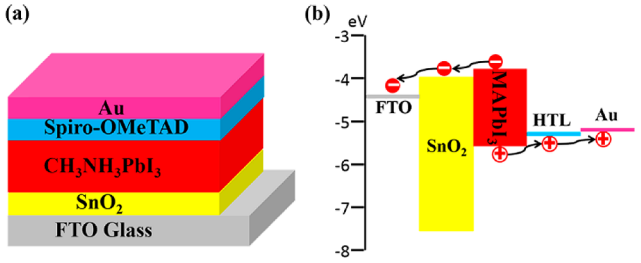

Figure 1. (a) Schematic view of the cell structure. (b) Energy band diagram of the perovskite solar cell, showing the separation and collection of photogenerated electrons and holes.

band diagram of our cells is shown in Figure 1b. Our low-temperature processed SnO_2 films have a nanocrystalline nature. This enables smooth and conformal coating of the SnO_2 thin layers on the FTO substrates. Figure 2a,b shows scanning electron microscopy (SEM) images of a FTO substrate fully covered with a SnO_2 nanocrystalline film at low and high magnifications, respectively. Figure 2a shows only the grains of the FTO substrate; however, at high magnification, the SnO_2 nanocrystallites are seen. Transmission electron microscopy (TEM) and selective area electron diffraction (SAED) images have confirmed that the low-temperature processed SnO_2 films are nanocrystalline (Figure 2b,c). X-ray photoelectron spectroscopy (XPS) measurement reveals that the composition of the films prepared by $SnCl_2{\cdot}2H_2O$ precursor at a low temperature is SnO_2 (Figure 3). The full XPS spectrum survey given in Figure 3a shows the presence of O and Sn. The binding energies of 487.11 and 495.56 eV correspond to the Sn $3d_{5/2}$ and Sn $3d_{3/2}$ peaks, respectively (Figure 3b). The main binding energy of 531.06 eV is attributed to the O 1s, which is the O^{2-} state in SnO_2 (Figure 3c). The higher binding energy can be assigned to the chemisorbed oxygen atoms or hydroxyl groups.[28,29] There is no residual Cl observed in our low-temperature processed SnO_2 films (Figure 3d). The low-temperature processed SnO_2 ETLs are fully compatible with the growth of $CH_3NH_3PbI_3$ perovskite absorbers. As shown in Figure 2e, the $CH_3NH_3PbI_3$ perovskite films coated on the SnO_2 ETLs have smooth surfaces and good coverage. The finished cells show good uniformity, as seen in the cross section SEM image (Figure 2f). The X-ray diffraction pattern shows that our $CH_3NH_3PbI_3$

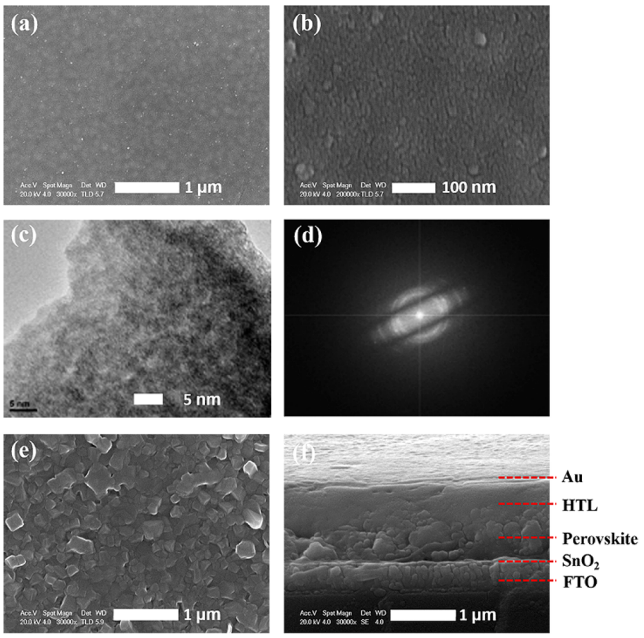

Figure 2. Top-view SEM images of a SnO_2 nanocrystalline film coated on FTO at (a) low and (b) high magnifications. (c) TEM and (d) SAED images of a SnO_2 nanocrystalline film. (e) Top-view SEM image of a perovskite $CH_3NH_3PbI_3$ film coated on the SnO_2 ETL. (f) Cross-sectional SEM image of the device.

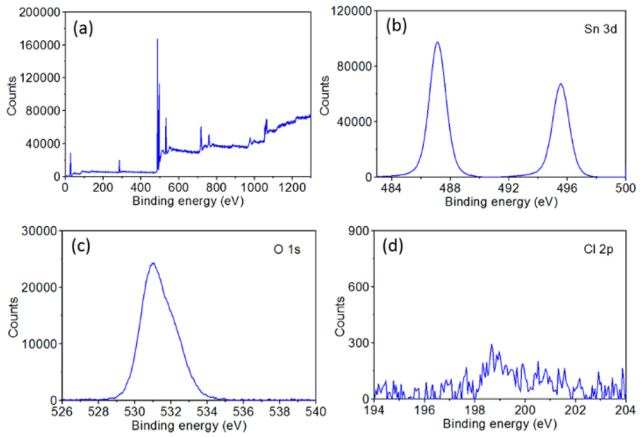

Figure 3. XPS spectra of (a) survey, (b) Sn 3d, (c) O 1s, and (d) Cl 2p peaks for a low-temperature solution-processed SnO_2 nanocrystalline film coated on a silicon substrate.

perovskite films are of similar quality to those reported in the literature (Figure S1).[4,30]

The thickness of the ETL can affect the cell's performance significantly. If an ETL is too thick, the cell will have a too high series resistance, which will reduce the J_{sc} and FF of the cell. If the ETL is too thin, there is a greater probability of direct contact between perovskite and FTO, which will make for less effective hole blocking and more serious carrier recombination. In our study, SnO_2 films with varying thicknesses were prepared by using solutions with different $SnCl_2{\cdot}2H_2O$ concentrations but a fixed spin rate and annealing temperature. The thickness increases as the $SnCl_2{\cdot}2H_2O$ concentration increases. We found that the cell performance first increases and then decreases as the $SnCl_2{\cdot}2H_2O$ concentration increases (Figure S2). The photovoltaic parameters of the cells using the SnO_2 ETLs prepared with different $SnCl_2{\cdot}2H_2O$ concentrations are

DOI: 10.1021/jacs.5b01994
J. Am. Chem. Soc. 2015, 137, 6730−6733

summarized in Table S1. We found that the optimum thickness for the SnO_2 ETL is about 60 nm, which is achieved by using a 0.1 M $SnCl_2{\cdot}2H_2O$ solution. We have further optimized the thicknesses of the absorber layer and the 2,2′,7,7′-tetrakis(*N*,*N*-di-*p*-methoxyphenylamine)-9,9′-spirobifluorene (spiro-OMeTAD) HTL. We found that an about 600 nm $CH_3NH_3PbI_3$ perovskite film followed by an about 500 nm HTL gives the best cell performance.

It is interesting to note that our low-temperature processed SnO_2 nanocrystalline films can improve the optical transmission properties of FTO substrates. Atomic force microscopy images show that the surface became smoother when the FTO substrate covered with a thin SnO_2 nanocrystalline film (Figure S3). The smoother surface should be beneficial to the light transmission. A FTO substrate coated with a 60 nm thick SnO_2 nanocrystalline film has shown better transmittance than a bare FTO substrate, excluding the measurement error (Figure 4a).

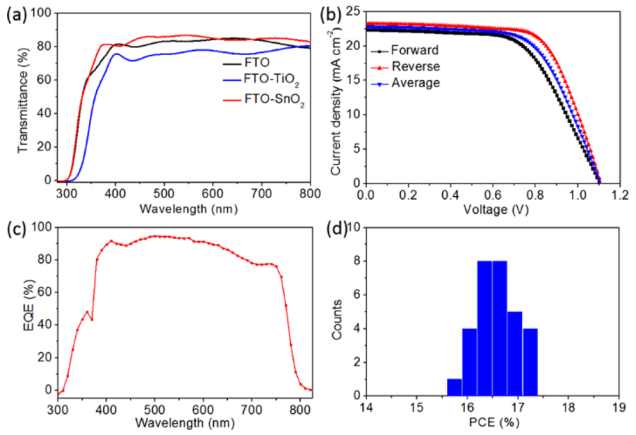

Figure 4. (a) Transmission spectra of FTO substrates without and with a compact 60 nm TiO_2 film or a 60 nm SnO_2 nanocrystalline film. (b) *J*–*V* curves of the best-performing perovskite $CH_3NH_3PbI_3$-based solar cell using a 60 nm SnO_2 ETL measured under reverse and forward voltage scans. (c) EQE spectrum of the best-performing cell using a SnO_2 ETL. (d) Histograms of PCEs measured for 30 cells using the SnO_2 ETLs.

For comparison, compact TiO_2 films with similar thickness are synthesized by using the method reported in the literature on the same batch of FTO substrates.[30] A representative transmission spectrum measured from these TiO_2-coated FTO substrates is shown in blue in Figure 4a. It is seen that the SnO_2 nanocrystalline film shows much higher transmission and a wider band gap than the TiO_2 compact film. It suggests an important way to achieve improved J_{sc} and, therefore, higher PCE for lead halide perovskite solar cells. It is noted that our perovskite solar cells exhibited hysteresis. It is therefore necessary to measure the cells with both reverse and forward scan directions. Figure 4b shows the *J*–*V* curves of the best-performing perovskite cell using a 60 nm SnO_2 ETL measured under both reverse and forward voltage scan directions with a scan rate of 0.1 V/s. The cell achieved a PCE of 17.21%, an V_{oc} of 1.11 V, a J_{sc} of 23.27 mA cm^{-2}, and a FF of 0.67 when measured under a reverse voltage scan. The same cell achieved a PCE of 14.82%, an V_{oc} of 1.11 V, a J_{sc} of 22.39 mA cm^{-2}, and a FF of 0.60 when measured under a forward voltage scan. The PCE, V_{oc}, J_{sc}, and FF values averaged from the *J*–*V* curves measured under different scan directions are 16.02%, 1.11 V, 22.83 mA cm^{-2}, and 0.64, respectively. All the photovoltaic parameters of this cell are summarized in Table 1. It is seen that only the FF showed a large reduction when the cell was

Table 1. Photovoltaic Parameters of the Best-Performing Cell Using a SnO_2 ETL under Different Scan Directions

	V_{oc} (V)	J_{sc} (mA cm^{-2})	FF	PCE (%)
forward	1.11	22.39	0.60	14.82
reverse	1.11	23.27	0.67	17.21
average	1.11	22.83	0.64	16.02

measured under the forward scan. The reduction on J_{sc} was small, and there was almost no reduction on V_{oc}. Therefore, the perovskite solar cells using the SnO_2 ETLs have a low hysteresis. It has been reported that SnO_2 has a high electron mobility.[25] The electron injection dynamic of the devices based on SnO_2 has been deeply investigated.[25] Therefore, perovskite solar cells using the SnO_2 ETLs should have a fast electron injection process and, therefore, a low carrier recombination. Our results suggest that the good charge transport at the ETL/perovskite interface could be partially responsible for the low hysteresis observed in our perovskite solar cells. This is consistent with recent reports on hysteresis-free perovskite solar cells.[31−33] In those solar cells, organic ETLs such as phenyl-C_{61}-butyric acid methyl ester and C_{60} were used to passivate traps and improve electron extraction and transportation. Figure 4c shows the external quantum efficiency (EQE) spectrum of the best-performing perovskite solar cell using a 60 nm SnO_2 ETL. The EQE spectrum shows a broad peak value of above 80% in the range from 400 to 760 nm. Some reports in the literature have shown that planar lead halide perovskite solar cells behave as p-i-n cells.[3,34−36] Our planar perovskite solar cells using the SnO_2 ETLs with the regular structure may also be considered p-i-n cells. Therefore, the series resistances (R_s) can be calculated by the diode equation.[16] The calculated R_s and the shunt resistances (R_{sh}) are 1.26 and 1840 Ω cm^2, respectively, for the best-performing cell using a SnO_2 ETL. The low R_s and high R_{sh} for the cell using SnO_2 ETL is partially attributed to the fact that SnO_2 has a high electron mobility. Furthermore, the SnO_2 ETL grown on FTO substrate has zero lattice mismatches, minimizing defects and reducing the carrier recombination at the FTO/ETL interface.

To check the reproducibility of the performance of the planar perovskite solar cells using the SnO_2 ETLs, we fabricated and measured 30 separate devices. The statistics of the PCEs measured under reverse voltage scan and a scan rate of 0.1 V/s are shown in Figure 4d. The average efficiency for the 30 cells using low-temperature solution-processed SnO_2 ETLs is 16.44%, with an V_{oc} of 1.09 V, a J_{sc} of 23.10 mA cm^{-2}, and a FF of 0.65. However, our best-performing perovskite solar cell, using a TiO_2 ETL with the same structure, has achieved a PCE of 15.17%, an V_{oc} of 1.06 V, a J_{sc} of 22.48 mA cm^{-2}, and a FF of 0.64, measured under the same scan direction and rate (Figure S4). The perovskite solar cells using the SnO_2 ETLs have higher average PCE, V_{oc}, J_{sc}, and FF. Figure S5 shows impedance spectra of the perovskite solar cells using different ETLs. The large semicircle in the low-frequency range is mainly attributed to recombination resistance (R_{rec}) and capacitance.[30] It shows that the cell using the SnO_2 ETL has a much higher R_{rec} and, therefore, much lower carrier recombiantion than the cell using the TiO_2 ETL. Therefore, the better photovoltaic performance can be mainly attributed to higher transmittance

DOI: 10.1021/jacs.5b01994
J. Am. Chem. Soc. 2015, 137, 6730−6733

of FTO substrate induced by the nanocrytalline SnO_2 ETL, wider band gap of SnO_2, and better hole blocking ability (lower carrier recombination). Good band edge matching could lead to reduced energy loss for photogenerated electrons and good blocking effects for holes. The latter results in reduced interfacial recombination.

In summary, we have demonstrated that low-temperature solution-processed SnO_2 is an excellent ETL material for high-performance perovskite solar cells. The average efficiency for 30 cells using low-temperature solution-processed SnO_2 ETLs is 16.44% under reverse voltage scan. The best-performing planar perovskite solar cell, using a nanocrystalline SnO_2 ETL, has achieved a PCE of 17.21% with a high V_{oc} of 1.11 V, a high J_{sc} of 23.27 mA cm^{-2}, and a FF of 0.67 under reverse voltage scan, much higher than those of our best reference cell using a TiO_2 ETL measured under the same scan conditions. The outstanding performance of the perovskite solar cells using the SnO_2 ETLs originates from the unique properties of nanocrystalline SnO_2 films such as good antireflection, high electron mobility, and wide band gap. This study opens a new direction to help push the performance of organic−inorganic lead halide perovskite solar cells to a higher level.

■ ASSOCIATED CONTENT

Ⓢ Supporting Information

Experimental method and additional figures and tables. The Supporting Information is available free of charge on the ACS Publications website at DOI: 10.1021/jacs.5b01994.

■ AUTHOR INFORMATION

Corresponding Authors

*gjfang@whu.edu.cn
*yanfa.yan@utoledo.edu

Notes

The authors declare no competing financial interest.

■ ACKNOWLEDGMENTS

The work at Wuhan University was supported by the National High Technology Research and Development Program (2015AA050601), the National Basic Research Program (No. 2011CB933300) of China, the National Natural Science Foundation of China (61376013, 91433203, J1210061), the Research Program of Wuhan Science & Technology Bureau (2013010501010141), and the Fundamental Research Funds for the Central Universities (2014202020207). The work at University of Toledo was supported by the U.S. Department of Energy SunShot Initiative under the Next Generation Photovoltaics 3 program (DE-FOA-0000990) and the Ohio Research Scholar Program.

■ REFERENCES

(1) Kojima, A.; Teshima, K.; Shirai, Y.; Miyasaka, T. *J. Am. Chem. Soc.* **2009**, *131*, 6050−6051.
(2) Kim, H. S.; Lee, C. R.; Im, J. H.; Lee, K. B.; Moehl, T.; Marchioro, A.; Moon, S. J.; Humphry-Baker, R.; Yum, J. H.; Moser, J. E.; Gratzel, M.; Park, N. G. *Sci. Rep.* **2012**, *2*, 591.
(3) Lee, M. M.; Teuscher, J.; Miyasaka, T.; Murakami, T. N.; Snaith, H. J. *Science* **2012**, *338*, 643−647.
(4) Burschka, J.; Pellet, N.; Moon, S. J.; Humphry-Baker, R.; Gao, P.; Nazeeruddin, M. K.; Gratzel, M. *Nature* **2013**, *499*, 316−319.
(5) Liu, M.; Johnston, M. B.; Snaith, H. J. *Nature* **2013**, *501*, 395−398.
(6) Im, J. H.; Jang, I. H.; Pellet, N.; Gratzel, M.; Park, N. G. *Nat. Nanotechnol* **2014**, *9*, 927−932.
(7) Zhou, H.; Chen, Q.; Li, G.; Luo, S.; Song, T. B.; Duan, H. S.; Hong, Z.; You, J.; Liu, Y.; Yang, Y. *Science* **2014**, *345*, 542−546.
(8) Jeon, N. J.; Noh, J. H.; Yang, W. S.; Kim, Y. C.; Ryu, S.; Seo, J.; Seok, S. I. *Nature* **2015**, *517*, 476−480.
(9) Nie, W.; Tsai, H.; Asadpour, R.; Blancon, J.-C.; Neukirch, A. J.; Gupta, G.; Crochet, J. J.; Chhowalla, M.; Tretiak, S.; Alam, M. A.; Wang, H.-L.; Mohite, A. D. *Science* **2015**, *347*, 522−525.
(10) National Renewable Energy Laboratory. Best Research-Cell Efficiencies, 2015; www.nrel.gov/ncpv/images/efficiency_chart.jpg.
(11) De Wolf, S.; Holovsky, J.; Moon, S.-J.; Löper, P.; Niesen, B.; Ledinsky, M.; Haug, F.-J.; Yum, J.-H.; Ballif, C. *J. Phys. Chem. Lett.* **2014**, *5*, 1035−1039.
(12) Xing, G.; Mathews, N.; Sun, S.; Lim, S. S.; Lam, Y. M.; Gratzel, M.; Mhaisalkar, S.; Sum, T. C. *Science* **2013**, *342*, 344−347.
(13) Yin, W. J.; Shi, T.; Yan, Y. *Adv. Mater.* **2014**, *26*, 4653−4658.
(14) Yin, W.-J.; Shi, T.; Yan, Y. *Appl. Phys. Lett.* **2014**, *104*, No. 063903.
(15) Ke, W.; Fang, G.; Wan, J.; Tao, H.; Liu, Q.; Xiong, L.; Qin, P.; Wang, J.; Lei, H.; Yang, G.; Qin, M.; Zhao, X.; Yan, Y. *Nat. Commun.* **2015**, *6*, 6700.
(16) Shi, J.; Dong, J.; Lv, S.; Xu, Y.; Zhu, L.; Xiao, J.; Xu, X.; Wu, H.; Li, D.; Luo, Y.; Meng, Q. *Appl. Phys. Lett.* **2014**, *104*, No. 063901.
(17) Zhu, Z.; Ma, J.; Wang, Z.; Mu, C.; Fan, Z.; Du, L.; Bai, Y.; Fan, L.; Yan, H.; Phillips, D. L.; Yang, S. *J. Am. Chem. Soc.* **2014**, *136*, 3760−3763.
(18) Christians, J. A.; Fung, R. C.; Kamat, P. V. *J. Am. Chem. Soc.* **2014**, *136*, 758−764.
(19) Zhao, Y.; Zhu, K. *J. Am. Chem. Soc.* **2014**, *136*, 12241−12244.
(20) Zhao, Y.; Nardes, A. M.; Zhu, K. *Appl. Phys. Lett.* **2014**, *104*, No. 213906.
(21) Zhao, Y.; Zhu, K. *J. Phys. Chem. C* **2014**, *118*, 9412−9418.
(22) Xiao, Z.; Bi, C.; Shao, Y.; Dong, Q.; Wang, Q.; Yuan, Y.; Wang, C.; Gao, Y.; Huang, J. *Energy Environ. Sci.* **2014**, *7*, 2619−2623.
(23) Wang, B.; Xiao, X.; Chen, T. *Nanoscale* **2014**, *6*, 12287−12297.
(24) Leijtens, T.; Eperon, G. E.; Pathak, S.; Abate, A.; Lee, M. M.; Snaith, H. J. *Nat. Commun.* **2013**, *4*, 2885.
(25) Tiwana, P.; Docampo, P.; Johnston, M. B.; Snaith, H. J.; Herz, L. M. *ACS Nano* **2011**, *5*, 5158−5166.
(26) Liu, D.; Kelly, T. L. *Nat. Photon.* **2013**, *8*, 133−138.
(27) Snaith, H. J.; Ducati, C. *Nano Lett.* **2010**, *10*, 1259−1265.
(28) Bob, B.; Song, T.-B.; Chen, C.-C.; Xu, Z.; Yang, Y. *Chem. Mater.* **2013**, *25*, 4725−4730.
(29) Kwoka, M.; Ottaviano, L.; Passacantando, M.; Santucci, S.; Czempik, G.; Szuber, J. *Thin Solid Films* **2005**, *490*, 36−42.
(30) Ke, W.; Fang, G.; Wang, J.; Qin, P.; Tao, H.; Lei, H.; Liu, Q.; Dai, X.; Zhao, X. *ACS Appl. Mater. Interfaces* **2014**, *6*, 15959−15965.
(31) Xiao, Z.; Dong, Q.; Bi, C.; Shao, Y.; Yuan, Y.; Huang, J. *Adv. Mater.* **2014**, *26*, 6503−6509.
(32) Bi, C.; Yuan, Y.; Fang, Y.; Huang, J. *Adv. Energy Mater.* **2014**, *4*, No. 1401616.
(33) Shao, Y.; Xiao, Z.; Bi, C.; Yuan, Y.; Huang, J. *Nat. Commun.* **2014**, *5*, 5784.
(34) Seo, J.; Park, S.; Chan Kim, Y.; Jeon, N. J.; Noh, J. H.; Yoon, S. C.; Seok, S. I. *Energy Environ. Sci.* **2014**, *7*, 2642−2646.
(35) Edri, E.; Kirmayer, S.; Henning, A.; Mukhopadhyay, S.; Gartsman, K.; Rosenwaks, Y.; Hodes, G.; Cahen, D. *Nano Lett.* **2014**, *14*, 1000−1004.
(36) Edri, E.; Kirmayer, S.; Mukhopadhyay, S.; Gartsman, K.; Hodes, G.; Cahen, D. *Nat. Commun.* **2014**, *5*, 3461.

DOI: 10.1021/jacs.5b01994
J. Am. Chem. Soc. 2015, 137, 6730−6733